Radiation Effects and Defects in Solids, Vol. 142, pp. 127–145
Reprints available directly from the publisher
Photocopying permitted by license only

PUSHING THE LIMITS OF CLASSICAL MODELING OF BOMBARDMENT EVENTS IN SOLIDS

REEMA CHATTERJEE and BARBARA J. GARRISON*

Department of Chemistry, The Pennsylvania State University, University Park, PA 16802, USA

(Received 5 September 1996; Revised 12 September 1996)

Bombardment of solids with keV atoms leads to violent collisions with subsequent ejection of target particles. This review discusses how classical molecular dynamics simulations designed to describe the bombardment events can give insight into microscopic processes where not only classical but also quantum effects such as electronic excitation and organic reactions play an important role. By incorporating a simple excitation/de-excitation model into the simulation, we have shown that collisional events are important to describe the distribution of excited state atoms measured experimentally. Molecular dynamics simulations employing a reactive many-body potential of small hydrocarbon molecules adsorbed on a metal surface predict the occurrence of various collision induced organic reactions prior to ejection. Lateral motion of particles in the region right above the surface plays an important role in signal enhancement. The calculations predict several processes such as direct molecular ejection, dissociation to fragments, unimolecular rearrangement and hydrogen abstraction reactions.

Keywords: Computer simulation; Molecular dynamics; Organic overlayers; Sputtering; Electronic effects

INTRODUCTION

The ability to model energetic particle bombardment of solids has grown enormously over the past thirty years. This growth has been spurred by developments in computer technology and in development of experiments that are able to obtain more and more detailed information about the system. For example, the early work of Harrison [1]

*Corresponding author.

of molecular dynamics simulations of single crystals was treated with some skepticism as there were not the detailed data for verification of the concepts from the simulation. Even our early work was to a large extent based on the theme "here is what comes out of the simulation" [2]. A few successful comparisons with detailed experimental data [3,4], however, provide the basis for using the simulations to enhance our knowledge of the fundamental processes that occur during particle bombardment. As evidenced by the articles in this issue, molecular dynamics simulations are now routinely used to understand the basic phenomena.

The molecular dynamics model is inherently based on classical mechanics. There are undoubtedly quantum processes occurring during particle bombardment. The challenge is to figure out when and where the quantum effects are important. In this paper we present examples of detailed comparisons of the simulations to experimental data and also examples of where the classical simulations can give insight into processes where quantum mechanics plays an important role.

METHODOLOGY

The basic molecular dynamics (MD) method consists of integrating Hamilton's equations of motion over some time interval to predict the resulting position and velocity of each atom in the system. The details of implementing the procedure are described in a book by Allen and Tildesley [5]. For particle bombardment we use a slab of atoms with an incident particle impinging on one surface of the slab. The integration is continued until each of the remaining atoms in the solid do not have sufficient energy to eject. The final positions, velocities and energetics of all the ejected atoms are used to obtain kinetic energy and angular distributions and the mass spectrum of the ejected species. The time evolution is used to extract important collisional events of relevant ejection mechanisms. Specifics of the implementation of the MD method to particle bombardment is found in the literature and will not be repeated here [6,7]. Of note is that a necessary element in any MD simulation is a potential energy surface (PES) which describes the energy and forces of the system for all possible configurations [8]. It is the quality of the PES that governs the reliability of the results of the MD simulations.

As evidenced by the presentations at this meeting, a large number of researchers have switched to many-body interaction potentials. Having a many-body potential, however, does not guarantee perfect results. To date there are only a handful of many-body potential energy surfaces that have been used extensively for a variety of simulations [8]. An example of a study that makes quantitative comparisons among the potentials is by Balamane *et al.* for Si systems [9]. The ability to use *ab initio* potentials, however, is beyond current computer capabilities for system sizes presented in many of the papers at this meeting. It is with some caution that we perform MD simulations for large reactive systems. Successes as judged by comparisons to experimental data though encourage us to move forward. Our favorite potentials [8] are the MD/MC-CEM potentials [10–12] for fcc metals although the Sandra EAM fcc potentials [13–15] have also been successfully used for many simulations, the Tersoff potential for Si [16], the Stillinger–Weber potential for Si [17] and Si–F [18,19] and the Brenner potential for hydrocarbons [20,21]. It is the Brenner potential that allows us to dream of using classical mechanics for organic reactions.

ATOMIC SOLIDS

MD simulations using many-body potentials have been implemented to examine the experimental energy and angular distributions of atomic species after keV ion bombardment of solids. As an initial calibration we examined fcc and diamond lattice systems. As shown in Fig. 1, the experimental energy distributions of Rh from Rh{111} are in excellent agreement with calculations using the EAM potential [13], while the calculated distribution using pair potentials peak at a significantly lower energy [22,23]. The energy resolved angular distributions of Ni from Ni{001} are shown in Fig. 2 [24]. In this case, MD simulations were done using the MD/MC-CEM potential [10–12]. The calculated distributions exhibit the same features and trends as the experimental distributions.

The excellent agreement between the experimental and calculated energy and angular distributions for fcc surfaces makes it attractive to use the information obtained from the simulations to obtain a microscopic view of the various bombardment events [24]. The calculations

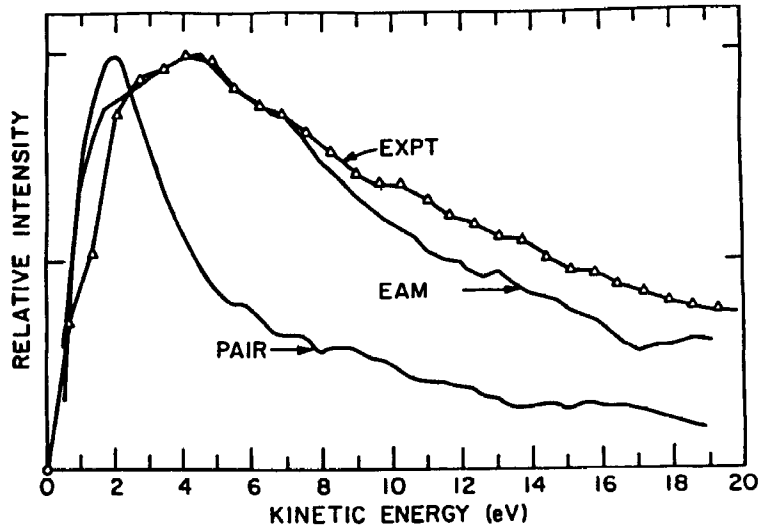

FIGURE 1 Experimental and calculated angle-integrated kinetic energy distributions of Rh from Rh{111}. In all cases, the curves are peak normalized (from Ref. [22]).

tell us that for the {001} surface the collision sequences are strongly dominated by the alignment of atomic motions inside the solid. The majority of ejected species originate from the first layer. Though the yield of second layer atoms is low, they are found to eject preferentially along the normal direction and are largely responsible for the intensity at $\theta \leq 10°$. The dominant mechanism of ejection is one in which particles eject due to collision with an atom from a layer below (Δ_1 mechanism). Collisions involving atoms in the same layer (Δ_0 mechanism) give rise to a shift in the peak position of the angular distributions.

MD simulations can also be used in structure elucidation of surfaces. The surface structure of GaAs{001} and metal overlayers on GaAs is of interest technologically. The experimentally obtained angular distribution of 20 eV Al^+ ejected after keV bombardment of a 0.3 monolayer of Al on GaAs{001} is shown in Fig. 3(c) [25]. The features in the angular distribution suggest placement of Al atoms on a (2×4) surface either $0.31a_0$ or $0.15a_0$ above the surface ($a_0 = 5.43$ Å) in the trough between two As_2 dimers. The angular distributions obtained from MD simulations using the Si potential developed by Tersoff [16], as shown in Figs. 3(a) and (b) for the two adsorption heights, are compared with

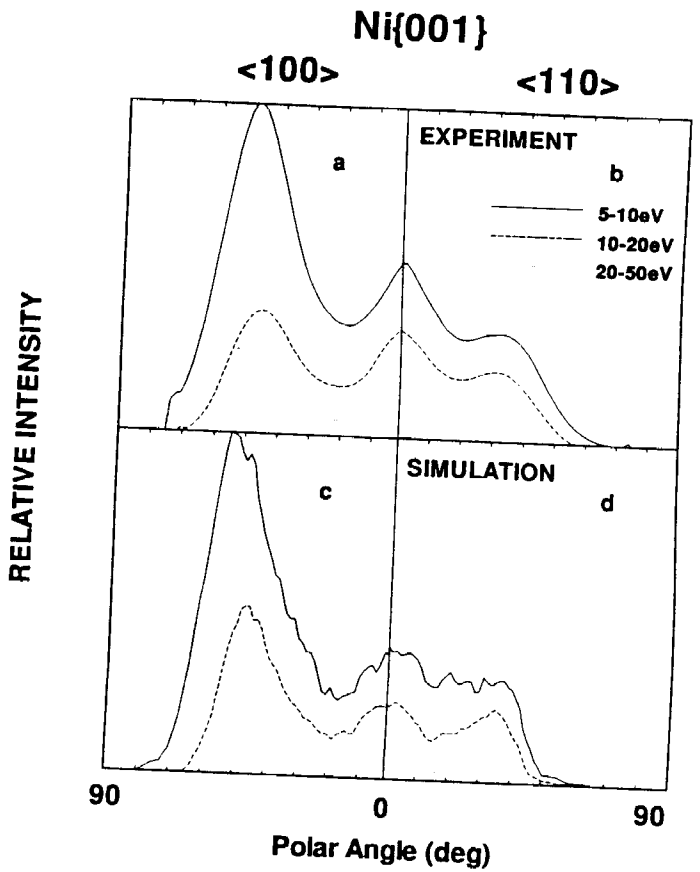

FIGURE 2 Experimental and calculated polar angle distributions of Ni from Ni{001} for three ranges of energies along the open ⟨100⟩ azimuth and closed packed ⟨110⟩ azimuth (from Ref. [24]).

the experimental distributions shown in Fig. 3(c). The similarity between Figs. 3(b) and (c) tells us the bonding position of Al is about $0.15a_0$ above the surface.

In simple systems, such as atomic solids, the collision mechanisms leading to ejection are well understood and we can determine the surface structure. Can we use MD simulations to explain more complex phenomena occurring during the bombardment process in different systems?

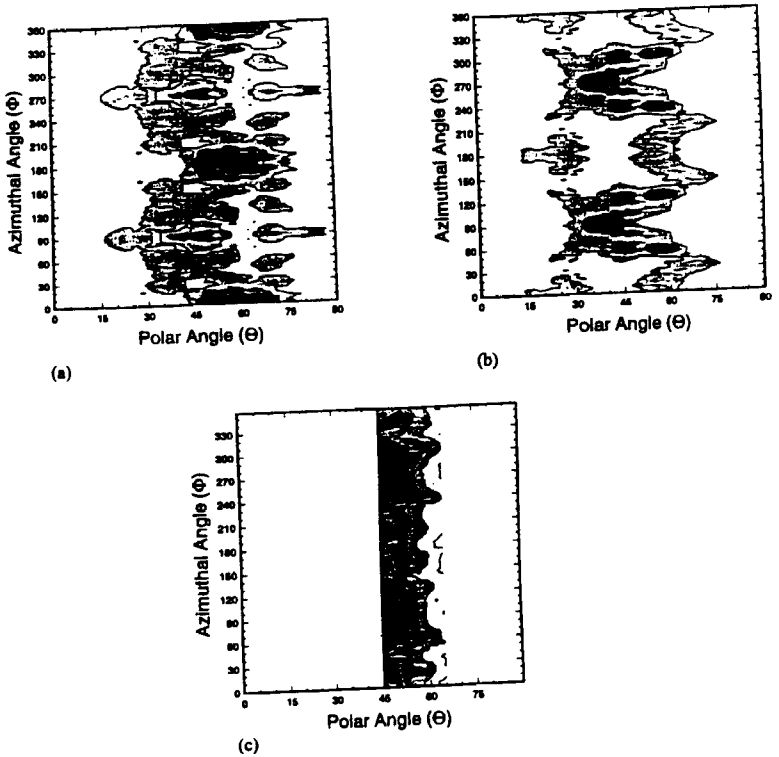

FIGURE 3 Angular distributions of adlayer Al atoms (from Ref. [25]). (a) Calculated distributions of 10–30 eV atoms desorbed from the $0.31a_0$ binding height model. (b) Calculated distributions of 10–30 eV atoms desorbed from the $0.15a_0$ binding height model. (c) Experimental distributions of 20 eV secondary Al^+ ions ejected from 0.3 ML Al deposited on GaAs{001}.

ELECTRONIC EXCITATIONS

The formation of atoms in excited electronic states subsequent to keV ion bombardment of metals has been of interest to further the basic understanding of inelastic processes in ion solid interactions. State selective detection using multiphoton ionization has been used to probe the $^4F_{9/2}$ ground state and the $^4F_{7/2}$ excited electronic state of Rh ejected after ion bombardment of Rh{100} [26]. As a preliminary analysis of the experimental data the ratio of the excited state ($N^* = {}^4F_{7/2}$) intensity to the ground state ($N = {}^4F_{9/2}$) intensity is plotted vs. $1/v_\perp$ as shown in

Fig. 4(a). For high velocities the results fit the Hagstrum de-excitation model [27]. At velocities corresponding to energies less than ~13 eV, however, the ratio of excited state to ground state intensity is independent of the perpendicular velocity, $v_\perp$.

In order to understand this effect we modeled the bombardment of Rh{001} [28]. The excitation process is assumed to occur when an encounter between two atoms becomes smaller than a critical threshold

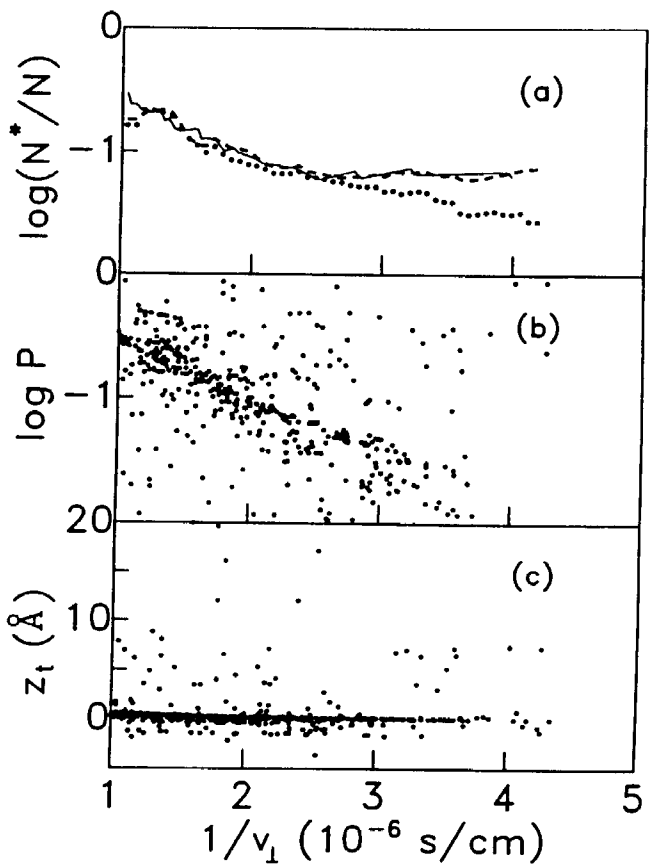

FIGURE 4 Results of electronic excitation calculations (from Ref. [30]). (a) Dashed line represents $\log(N^*/N)$ vs $1/v_\perp$ as predicted by simulations for particles ejected with $\theta < 20°$. Dotted line represents the reevaluation of $\log(N^*/N)$ with the omission of atoms last excited above the surface. Solid line represents the experimental results for atoms with $\theta < 10°$. (b) Excitation probabilities for individual atoms as predicted by the simulations. (c) Height at which an atom was last excited, z_t.

distance, r_{th}, yielding an initial excitation probability P_0. After excitation, the excitation probability is subjected to a time dependent decay with a characteristic lifetime τ

$$dP/dt = -P/\tau.$$

It is assumed that this decay is a result of coupling between the excited atom and the electrons in the solid. In our calculations [29] τ is defined in terms of the electron density of the atoms in the solid, which can be obtained from the EAM potential.

Simulating electronic excitations now involves combining molecular dynamics simulation with the above electronic excitation model [28]. The molecular dynamics simulations yield $N_t(v, \theta, \phi)$ the total number of atoms ejected with velocity v and polar and azimuthal angles of θ and ϕ. The electronic excitation model gives excitation probabilities for these atoms. The number of atoms in the excited state is obtained by

$$N^*(v, \theta, \phi) = N_t(v, \theta, \phi)P(v, \theta, \phi).$$

Assuming that the first excited state and the ground state represent nearly the entire population, the number of ground state atoms is given by

$$N(v, \theta, \phi) = N_t(v, \theta, \phi)\{1 - P(v, \theta, \phi)\}.$$

The ratio of the excited state population (N^*) to the ground state population (N) obtained from experiments and theoretical prediction as presented in Fig. 4(a) show remarkable similarity [30]. A linear relation between $\log(N^*/N)$ and $1/v_\perp$ is observed at high velocities [31]. At low velocities N^*/N becomes independent of $v_\perp$. The excitation probabilities as shown in Fig. 4(b) decay exponentially with $1/v_\perp$. There are ejected atoms, however, whose excitation probabilities are quite high.

Examining the excitation history of these atoms, we observe that these atoms were last excited with other atoms some distance ($\sim$ 1–20 Å) above the surface (Fig. 4(c)). These calculations show that the enhanced excitation probability in the low velocity regime arises from the atoms that are excited above the surface and exhibit relatively little de-excitation. Since slow moving atoms that are excited at the surface are almost completely de-excited, the atoms excited above the surface

contribute significantly to the total excitation probability in the low velocity region. This is evident in Fig. 4(a) where omission of atoms with last excitation above the surface yields a result dependent on $1/v_\perp$ even at low velocities (dotted line).

We have shown how the collisional excitation model in conjunction with molecular dynamics simulations can be used to identify quantum effects. A detailed analysis of all the events in the MD simulation illustrates the importance of excited atoms produced by collisional excitations a few angstroms above the surface. This basic approach of incorporating simple quantum models [32] into the MD simulations shows promise for microscopic examination of quantum effects in sputtering.

BAND STRUCTURE EFFECTS

Shown in Fig. 5 are energy distributions of a^3F_4 ground state and a^3D_3 excited state Ni atoms ejected from an ion-bombarded Ni{001} crystal [33]. A comparison of the distribution with those obtained from simulations (dotted lines) show that the shapes of the distributions match only with those observed for the $^3D_3$ state. Moreover, the experimental results show that the population of the excited $^3D_3$ state is higher than that of the ground $^3F_4$ state. This can be explained by the fact that the Ni band structure is D-like in character and the observed enhanced D

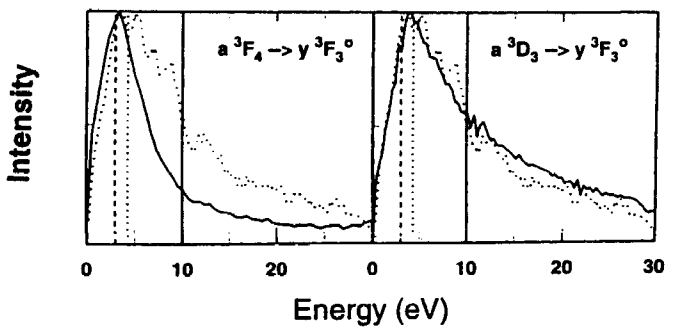

FIGURE 5 Kinetic energy distribution of a^3F_4 ground state and a^3D_3 excited state Ni atoms from Ni{001} (solid lines). The dotted lines represent the distributions predicted by MD simulations (from Ref. [33]).

'state intensity is a direct consequence of being the predominant bonding state of the metal. The MD simulations were done using the MD/MC-CEM potential energy function fit to the bulk cohesive energy for Ni. The calculated result represents the predominant state in the metal which was crucial in explaining the population inversion observed experimentally.

Subsequent to this investigation several other anomalous systems have been measured. Berthold and Wucher measured the energy distribution of the $^2D_{5/2}$ (3.75 eV) excited state of Ag and found that it peaked at a lower energy than the ground state ($^2S_{1/2}$) [34]. Vandeweert *et al.* have measured populations of excited states of 1.5–2.0 eV excitation energy in Ni and Co and have found populations as high as 20% of the ground state [35]. Obviously there is something interesting taking place. Can MD simulations help us understand the phenomena? The simulations certainly played an important role in the initial interpretation of the Ni data [33].

ORGANIC REACTIONS

The Brenner CH potential has been used in MD simulations to study collision induced reactions of organic films adsorbed on a Pt{111} surface [36]. To realistically describe the Pt C and Pt–H interactions, pairwise potential functions have been merged with Brenner's reactive CH potential in such a way as to describe the binding site energetics and adsorbate geometries of various small hydrocarbons adsorbed on Pt [36]. Both the structure and binding site of each adsorbate is assumed prior to the beginning of the simulation. As the collision cascade evolves, reactions occurring among the substrate atoms, the substrate and adsorbate atoms and between individual adsorbate atoms can be followed in time with the MD calculations.

MD simulations of 500 eV Ar bombardment of organic films such as CH, CH_2, CH_3, C_2H_3, C_3H_7 and C_5H_9 on a Pt{111} surface show that the species created during the collision event not only originate from dissociation of single adsorbates but also from recombination of two adsorbates. Several collision induced processes, as predicted by the calculations, are direct molecular ejection, dissociation to fragments, rearrangement reactions and hydrogen abstraction reactions.

Simulations also predict the occurrence of considerable lateral motion of particles in the region right above the surface [37]. For smaller adsorbates such as CH_x, dominant species are the intact adsorbates or a H atom. Larger molecules that extend far above the surface are exposed to more collisions from the laterally moving particles and consequently undergo more fragmentation and the dominant ejected species is usually not the original adsorbate [38]. The lateral motion of organic fragments readily identified in simulations were not recognized earlier.

Unimolecular rearrangement and fragmentation of C_2H_3 yielding HCCH is shown in Fig. 6. This example shows how an internally excited C_2H_3 molecule ejects, rearranges to $HCCH_2$ and dissociates to give stable HCCH and H atom, all within 1 picosecond [36]. The MD approach yields internal energies of all the molecules and it is relatively

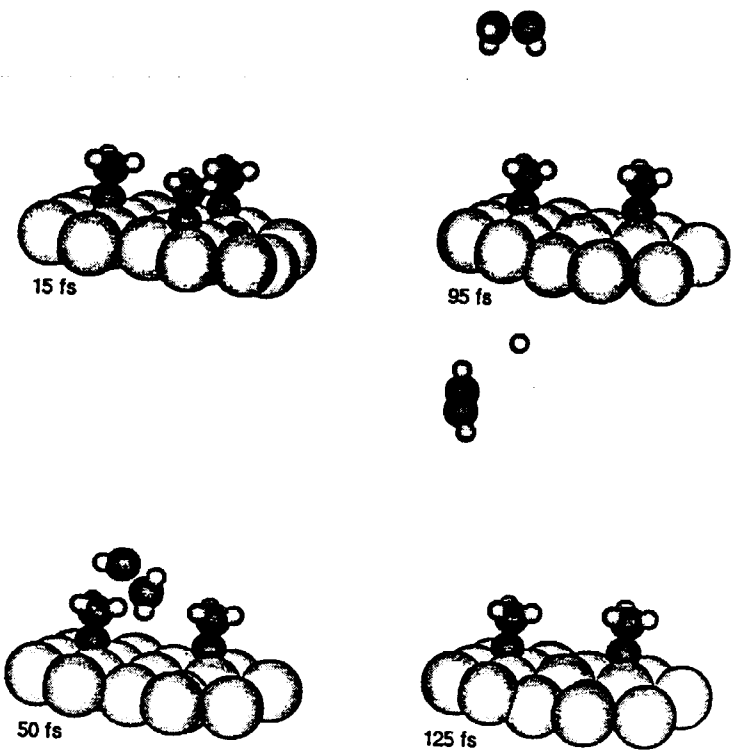

FIGURE 6 Unimolecular rearrangement and fragmentation of C_2H_3 yielding HCCH (from Ref. [36]).

straightforward to monitor how these molecules evolve and/or fragment with time. Although the potential energy function used to describe the hydrocarbon interactions in these calculations may not predict the correct energy barrier for this reaction, the potential does allow classical dynamics simulation to be used in the qualitative study of such unimolecular dissociation/rearrangement type collision induced reactions.

Intermolecular reactions can be depicted by the hydrogen abstraction mechanism which accounts for 66% of the ejected H_2 in the simulations [39]. The two main abstraction mechanisms seen during the formation of H_2 are shown in Fig. 7. In the predominant mechanism, scheme 1, a H atom emitted from a C_2H_3 molecule moves laterally on the surface and reacts with another H atom on a undisturbed C_2H_3 molecule to form a H_2 molecule. In scheme 2, a C_2H_3 gets bumped such that one of its H atoms interacts with a H atom on a neighboring C_2H_3. Similar hydrogen abstraction type mechanisms also occur during other reactions to eject different molecular species, varying from H_2 to $Pt_nC_yH_2$. In experimentally obtained SIMS (secondary ion mass

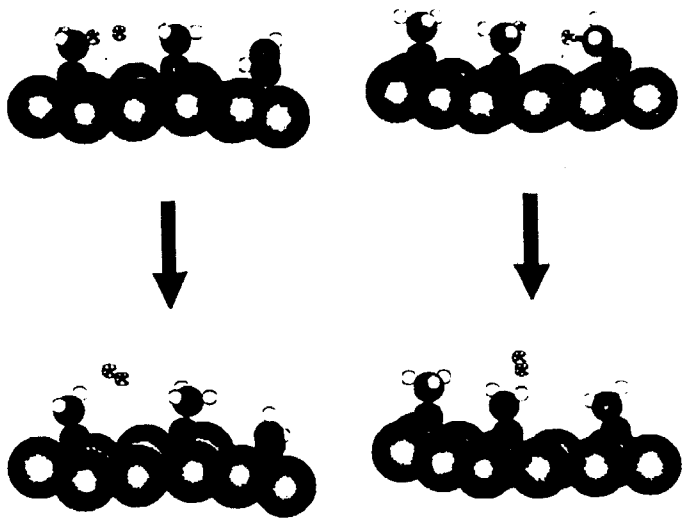

FIGURE 7 Two pathways for H abstraction. The light gray, black and white spheres represent Pt, C, and H atoms. The H atoms that eventually form H_2 are marked with stars (from Ref. [39]).

spectrometry) spectra of organic molecules, the peaks of the molecular ions $(M \pm H)^{\pm}$ are often quite intense [40]. Several mechanisms have been ventured for the origin of these molecular ions. The "preformed ion" mechanism postulates that the ions are created prior to the ion bombardment event that ejected them [41,42]. Reduction reactions have been proposed to occur through electron transfer alone or electron transfer with hydrogen attachment to the molecular ion [41–44]. Until now it was believed that the H atoms emanated either from the substrate matrix, such as glycerol often used in FAB, or from decomposition of the molecular ion itself [41,44]. In the particular example of organic films adsorbed on a transition metal, it is not easy to imagine which of the above events lead to the formation of $(M \pm H)^{\pm}$. Although classical dynamics simulations do not take into account the presence of electrons, these simulations do suggest an alternate source of hydrogen and the possible occurrence of a similar hydrogen abstraction type mechanism for the formation of these molecular ions.

The identification of how molecular reactions proceed during keV particle bombardment should aid in relating the structure of molecular solids to the peaks observed in the mass spectra. It is encouraging that MD simulations with the use of a suitable reactive potential can actually predict several reaction pathways. Mechanisms such as lateral motion, unimolecular rearrangement/fragmentation and above all the H_2 abstraction where electronic and quantum effects play an important role can now be identified by classical dynamics. The strength of this approach lies in the microscopic detail that comes from the atomic positions as a function of time.

BINDING ENERGY EFFECT

MD calculations of high energy bombardment of a pentylidyne (C_5H_9) film adsorbed on a platinum surface have been done to elucidate the effect of the bond strength of the adsorbate with the surface [45]. As shown in Fig. 8(b), if an energetic fragment strikes a molecule bound to the surface by 2.7 eV, bond rupture occurs near the point of contact and fragments are ejected. If, on the other hand, the adsorbate bond strength is only 0.6 eV, the whole molecule is more easily propelled from the surface as shown in Fig. 8(c). A similar effect has been seen

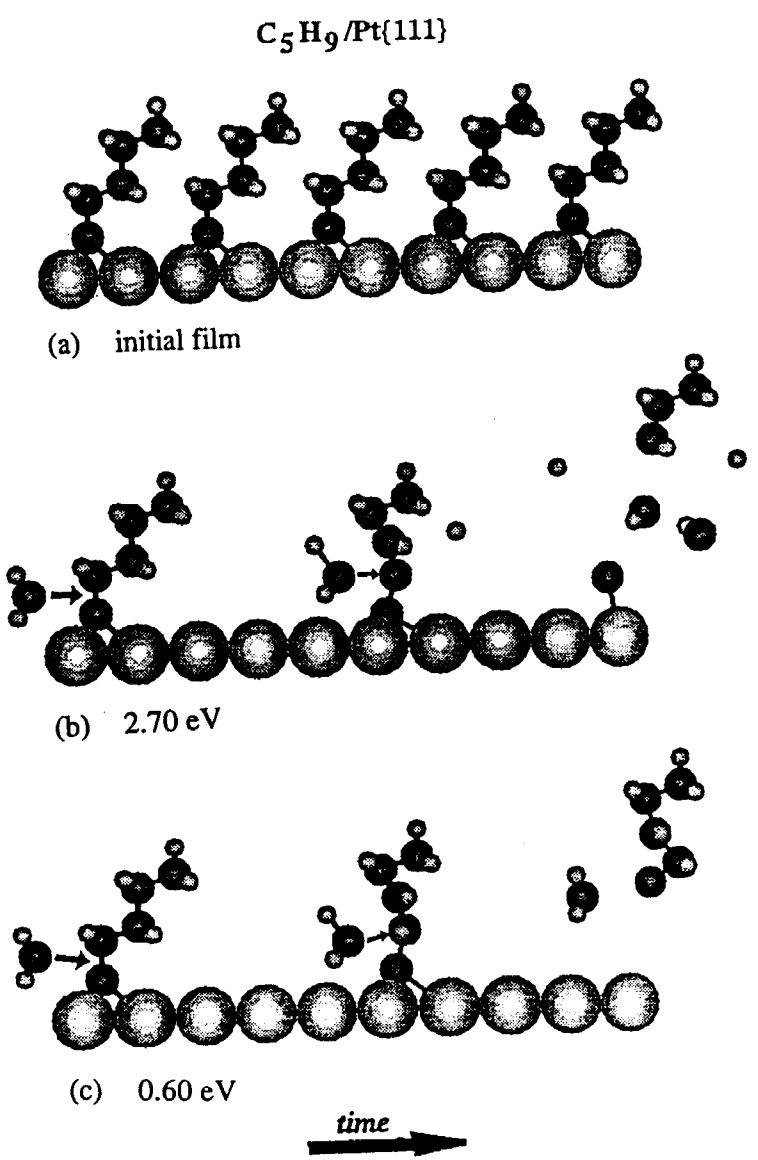

FIGURE 8 C_5H_9 bound in fcc threefold site on Pt{111} (from Ref. [38]). (a) Initial array. (b) Scenario for ejection of fragment from C_5H_9 film bound by 2.7 eV on Pt{111}. (c) Scenario for ejection of parent molecule from C_5H_9 film bound by 0.6 eV on Pt{111}. In (b) and (c) the time evolution is from left to right across the crystal.

experimentally in the molecular ion yield of small peptides adsorbed on a surface [46]. For combinatorial libraries of peptides covalently bound to polystyrene beads, no parent peak was observed. Yet when the peptide was physisorbed to the bead by clipping the covalent linker bond with an acid vapor, the parent peak appeared in abundance.

It is assumed that ejection occurs due to collisions from the bulk that knock off molecular species on the surface. Analytical models for the collision cascade theory predict that the ejection yield is proportional to the reciprocal of the binding energy [47]. The signal enhancement of the parent peak (factor of 9) in the simulations is much higher than that expected from the ratio of the binding energies (2.7/0.6 = 4.5). This extra enhancement is due to laterally moving species, which can 'pull off' the weakly bound adsorbate molecule. The total yield of emitted particles increases as the angle of incidence is changed from 0° to 45° in the case of the tightly bound adsorbate. The main effect of the off-normal angle of incidence is to increase the initial fragmentation of the film and not to enhance the molecular ejection. Fragments created by the beam can then move laterally across the surface and further fragment other molecules (Fig. 8(b)). The results illustrate the role played by laterally moving fragments in signal enhancement of the parent-peak in the case of weakly bound adsorbates and that of the fragment peak in adsorbates bound strongly to the surface. These calculations also illustrate how customizing the substrate-analyte linker to get different bond strengths can enhance the molecular ion yields in experiments.

SUBSTRATE MASS EFFECT

Calculations of high energy bombardment of pentylidyne (C_5H_9) film adsorbed on Pt{111} and hydrogen terminated C{111} were performed to see the effect of substrate mass on the ejection yield [45]. The results show that the yields from a C substrate is much less than that from a Pt substrate. The difference in yields observed from ^{195}Pt and ^{12}C matrices is due to the inability of diamond to redirect the momentum of the ^{40}Ar beam in the upward direction. The C atoms are too light to turn around the momentum of Ar beam in an upward direction. This is evidently clear when we compare the yields with the substrate masses arbitrarily switched (^{195}C, ^{12}Pt) but the crystal structure and interaction potentials

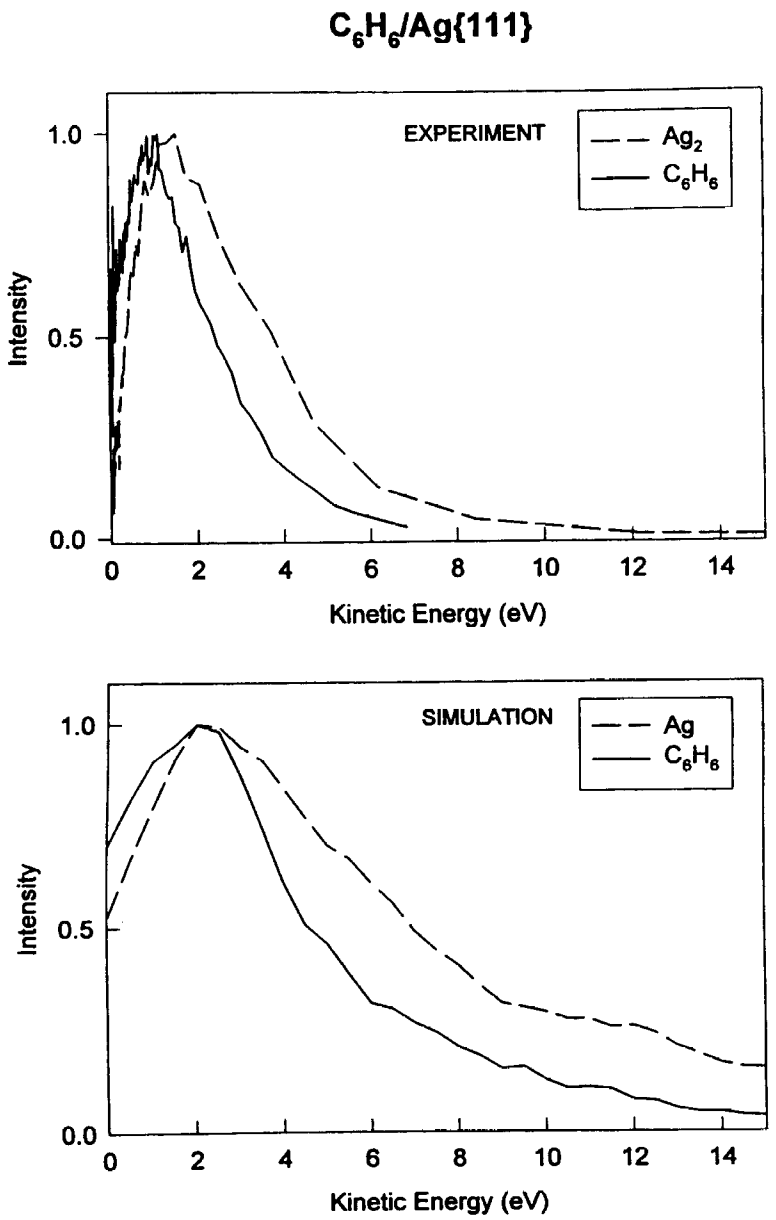

FIGURE 9 Experimental and calculated kinetic energy distributions of benzene and silver from C_6H_6/Ag{111}.

are left unaltered. Both the crystal structures exhibit a large mass effect in the calculated yield. Metals therefore provide an excellent substrates for SIMS (secondary on mass spectrometry) and using higher mass substrates can help to increase the yield. It is crucial to realize that it is easier to pinpoint such effects in simulations by cleverly changing various parameters which might not be realistically possible in experiments.

MOLECULAR DESORPTION

The kinetic energy distributions of neutral benzene and silver ejected after ion bombardment of C_6H_6/Ag{111} are shown in Fig. 9. The experiments were done with submonolayer coverage of benzene on Ag{111} (1 L exposure) at 120 K [48]. The silver dimer distributions were measured, as the monomer distributions would have contributions from dimer fragmentation. The simulations were done using the Brenner potential to describe the interactions of the C and H atoms [49]. A pair potential was used for the interaction between Ag and C, H atoms. The silver and benzene distributions show similar trends in the experiment and simulation. In both the cases the energy distributions for benzene falls off faster at higher energies compared to that of silver. In the experimental result, the peak in the benzene distribution is shifted to lower values compared to that of silver. This is not seen in the simulations as presently the CH potential cannot take into account intermolecular interactions. These initial findings pave the way for further studies to investigate molecular desorption mechanisms.

Continued efforts aimed at modeling spectra of alkane thiols adsorbed on metal surfaces are given in another paper in this issue [50]. We are optimistic that a thorough interpretation of the experimental data can be made even though classical mechanics would not be presumed to be applicable to chemical reactions.

CONCLUSION

A diverse range of collision induced processes have been discussed above. MD simulations using classical approximations have been

successfully used to model atomic collisions, electronic excitations, hydrocarbon reactions and molecular desorption. We have now come a long way from the initial days of establishing how classical modeling is a useful tool in understanding bombardment events in solids. While mechanistic insight from collision induced atomic and molecular motion, substrate/projectile mass effects, substrate–adsorbate binding energy effect are some of the phenomena one would try to understand using molecular dynamics, we have shown how obtaining a microscopic understanding of electronic excitations, band structure effects, organic reactions like hydrogen abstraction or unimolecular rearrangement/fragmentation are only possible by carefully and cleverly using classical dynamics to get an insight into processes where quantum effects are important.

Acknowledgments

The support from the National Science Foundation, Office of Naval Research, and IBM-SUR Program is gratefully acknowledged. Also, we would like to acknowledge D.N. Bernardo, R. Bhatia, D.W. Brenner, S.W. Rosencrance, D.E. Sanders, R.S. Taylor, and N. Winograd for their various contributions to this work.

References

[1] W.L. Gay and D.E. Harrison, Jr., *Phys. Rev.* **135A**, 1780 (1965).
[2] D.E. Harrison, Jr., P.W. Kelly, B.J. Garrison and N. Winograd, *Surf. Sci.* **76**, 311 (1978).
[3] S.P. Holland, B.J. Garrison and N. Winograd, *Phys. Rev. Lett.* **43**, 220 (1979).
[4] S.P. Holland, B.J. Garrison and N. Winograd, *Phys. Rev. Lett.* **44**, 756 (1980).
[5] M.P. Allen and D.J. Tildesley, *Computer Simulation of Solids* 1987, Clarendon Press, Oxford.
[6] B.J. Garrison, P.B.S. Kodali and D. Srivastava, *Chemical Reviews* **96**, 1327 (1996).
[7] D.E. Harrison, Jr., *CRC Crit. Rev. Solid State Mater. Sci.* **14**, 51 (1988).
[8] B.J. Garrison and D. Srivastava, *Ann. Rev. Phys. Chem.* **46**, 373 (1995).
[9] H. Balamane, T. Halicioglu and W.A. Tiller, *Phys. Rev. B* **46**, 2250 (1992).
[10] M.S. Stave, D.E. Sanders, T.J. Raeker and A.E. DePristo, *J. Chem. Phys.* **93**, 4413 (1990).
[11] T.J. Raeker and A.E. DePristo, *Int. Rev. Phys. Chem.* **10**, 1 (1991).
[12] C.L. Kelchner, D.M. Halstead, L.S. Perkins, N.M. Wallace and A.E. DePristo, *Surf. Sci.* **310**, 425 (1994).
[13] S.M. Foiles, M.I. Baskes and M.S. Daw, *Phys. Rev. B* **33**, 7983 (1986).
[14] M.S. Daw and M.I. Baskes, *Phys. Rev. B* **29**, 6443 (1984).
[15] M.S. Daw and M.I. Baskes, *Phys. Rev. Lett.* **50**, 1285 (1983).
[16] J. Tersoff, *Phys. Rev. B* **38**, 9902 (1988).
[17] F.H. Stillinger and T.A. Weber, *Phys. Rev. B* **31**, 5262 (1985).

[18] F.H. Stillinger and T.A. Weber, *Phys. Rev. Lett.* **88**, 5123 (1988).
[19] F.H. Stillinger and T.A. Weber, *Phys. Rev. Lett.* **62**, 2144 (1989).
[20] D.W. Brenner, *Phys. Rev. B* **42**, 9458 (1990).
[21] D.W. Brenner, J.A. Harrison, C.T. White and R.J. Colton, *Thin Solid Films* **206**, 220 (1991).
[22] B.J. Garrison, N. Winograd, D.M. Deaven, C.T. Reimann, D.Y. Lo, T.A. Tombrello, D.E. Harrison, Jr. and M.H. Shapiro, *Phys. Rev. B* **37**, 7197 (1988).
[23] B.J. Garrison, K. Walzl, M. El-Maazawi, N. Winograd, C.T. Reimann and D.M. Deaven, *Rad. Eff. Def. in Solids* **109**, 287 (1989).
[24] S.W. Rosencrance, J.S. Burnham, D.E. Sanders, C. He, B.J. Garrison and N. Winograd, *Phys. Rev. B* **52**, 6006 (1995).
[25] J.S. Burnham, D.E. Sanders, C. Xu, R.M. Braun, S.H. Goss, K.P. Caffey, B.J. Garrison and N. Winograd, *Phys. Rev. B* **53**, 9901 (1996).
[26] N. Winograd, M. El-Maazawi, R. Maboudian, Z. Postawa, D.N. Bernardo and B.J. Garrison, *J. Chem. Phys.* **96**, 6314 (1992).
[27] H.D. Hagstrum, *Phys. Rev.* **96**, 336 (1954).
[28] D.N. Bernardo, M. El-Maazawi, R. Maboudian, Z. Postawa, N. Winograd and B.J Garrison, *J. Chem. Phys.* **97**, 3846 (1992).
[29] R. Bhatia and B.J. Garrison, *J. Chem. Phys.* **100**, 8437 (1994).
[30] D.N. Bernardo, R. Bhatia and B.J. Garrison, *Comp. Phys. Comm.* **80**, 259 (1994).
[31] Parameters in the model were chosen to reproduce the experimental slope and intercept in this region.
[32] M.H. Shapiro and J. Fine, *Nucl. Instrum. Methods B* **44**, 43 (1989).
[33] C. He, Z. Postawa, S.W. Rosencrance, R. Chatterjee, B.J. Garrison and N. Winograd, *Phys. Rev. Lett.* **75**, 3950 (1995).
[34] W. Berthold and A. Wucher, *Phys. Rev. Lett.* **76**, 2181 (1996).
[35] E. Vandeweert, P. Lievens, V. Philipsen, W. Bouwen, P. Thoen, H. Weidele, R.E. Silverans, *Proc. 8th Symp. on Res. Ion. Spec. and its Appl.*, Penn State, July 1996 and *Phys. Rev. Lett.*, in press.
[36] R.S. Taylor and B.J. Garrison, *Langmuir* **11**, 1220 (1995).
[37] R.S. Taylor and B.J. Garrison, *Int. J. of Mass. Spec. and Ion. Proc.* **143**, 225 (1995).
[38] R.S. Taylor and B.J. Garrison, *Chem. Phys. Lett.* **230**, 495 (1994).
[39] R.S. Taylor and B.J. Garrison, *J. Am. Chem. Soc.* **116**, 4465 (1994).
[40] J.C. Vickerman, A. Brown and N.M. Reed, Eds., *Secondary Ion Mass Spectrometry Principles and Applications* (Oxford Univ. Press, Oxford, 1989) pp. 1–71, 149–243.
[41] L.D. Detter, O.W. Hand, R.G. Cooks and R.A. Walton, *Mass Spectrom. Rev.* **7**, 465 (1988).
[42] S.J. Pachuta and R.G. Cooks, *Chem. Rev.* **87**, 647 (1987).
[43] J. Sunner, A. Morales and P. Kebarle, *Int. J. Mass Spectrom. Ion Processes* **86**, 169 (1988).
[44] D.H. Williams, A.F. Findeis, S. Naylor and B.W. Gibson, *J. Am. Chem. Soc.* **109**, 1980 (1987).
[45] R.S. Taylor, C.L. Brummel, N. Winograd, B.J. Garrison and J.C. Vickerman, *Chem. Phys. Lett.* **233**, 575 (1995).
[46] C.L. Brummel, I.N.W. Lee, Y. Zhou, S.J. Benkovic and N. Winograd, *Science* **233**, 399 (1994).
[47] P. Sigmund, *Phys. Rev.* **184**, 383 (1969).
[48] R. Chatterjee, D. Riederer, Z. Postawa, B.J. Garrison and N. Winograd, *Proc. 8th Symp. on Res. Ion. Spec. and its Appl., Penn State, July 1996*, in press.
[49] R. Chatterjee, N. Winograd and B.J. Garrison, to be published. The Ag-C and Ag-H potentials are described by Lennard–Jones (12,6) functional forms. Using the same definition of σ as in Ref. 36 (i.e. σ is the equilibrium separation, not the distance at which the potential is zero), for Ag-C, $\varepsilon = 0.5\,\text{eV}$ and $\sigma = 2.3\,\text{Å}$ and for Ag-H, $\varepsilon = 0.083\,\text{eV}$ and $\sigma = 2.3\,\text{Å}$.
[50] K.S.S. Liu, J.C. Vickerman and B.J. Garrison, *Rad. Effects*, this issue.